Increased magnetic damping in ultrathin films of Co_2FeAl with perpendicular anisotropy

Y. K. Takahashi, Y. Miura, R. Choi, T. Ohkubo, Z. C. Wen, K. Ishioka, R. Mandal, R. Medapalli, H. Sukegawa, S. Mitani, E. E. Fullerton, and K. Hono

Citation: Appl. Phys. Lett. **110**, 252409 (2017); doi: 10.1063/1.4989379
View online: https://doi.org/10.1063/1.4989379
View Table of Contents: http://aip.scitation.org/toc/apl/110/25
Published by the American Institute of Physics

Increased magnetic damping in ultrathin films of Co_2FeAl with perpendicular anisotropy

Y. K. Takahashi,[1,a)] Y. Miura,[1,2,3] R. Choi,[4] T. Ohkubo,[1] Z. C. Wen,[1] K. Ishioka,[5] R. Mandal,[1] R. Medapalli,[4] H. Sukegawa,[1] S. Mitani,[1] E. E. Fullerton,[4] and K. Hono[1]
[1]*Research Center for Magnetic and Spintronic Materials, National Institute for Materials Science, 1-2-1 Sengen, Tsukuba 305-0047, Japan*
[2]*Electrical Engineering and Electronics, Kyoto Institute of Technology, Kyoto 606-8585, Japan*
[3]*Center for Spintronics Research Network (CSRN), Osaka University, Toyonaka 560-8531, Japan*
[4]*Center for Memory and Recording Research, University of California San Diego, 9500 Gilman Drive, La Jolla, California 92093-0401, USA*
[5]*Research Center for Advanced Measurement and Characterization, National Institute for Materials Science, 1-2-1 Sengen, Tsukuba 305-0047, Japan*

(Received 3 March 2017; accepted 4 June 2017; published online 22 June 2017)

We estimated the magnetic damping constant α of Co_2FeAl (CFA) Heusler alloy films of different thicknesses with an MgO capping layer by means of time-resolved magneto-optical Kerr effect and ferromagnetic resonance measurements. CFA films with thicknesses of 1.2 nm and below exhibited perpendicular magnetic anisotropy arising from the presence of the interface with MgO. While α increased gradually with decreasing CFA film thickness down to 1.2 nm, it was increased substantially when the thickness was reduced further to 1.0 nm. Based on the microstructure analyses and first-principles calculations, we attributed the origin of the large α in the ultrathin CFA film primarily to the Al deficiency in the CFA layer, which caused an increase in the density of states and thereby in the scatterings of their spins. *Published by AIP Publishing.*
[http://dx.doi.org/10.1063/1.4989379]

Spin transfer torque magnetoresistive random access memories (STT-MRAMs), consisting of arrays of magnetic tunneling junctions (MTJs), have received much attention as a potential replacement of semiconductor memories because of their non-volatility, high speed operation, low power consumption, and scalability.[1] Nanometer-scale MTJs require high thermal stability and low current density (J_c) for the magnetization switching by STT, which can be realized by using materials with high perpendicular magnetic anisotropy (PMA), high spin polarization (P), and low magnetic damping constant (α) as the ferromagnetic electrodes, according to the Slonczewski theory.[2]

Co_2FeAl (CFA) Heusler alloys are one of the attractive ferromagnetic electrode materials due to the high spin polarization,[3,4] high Curie temperature of 1000 K (Ref. 5), and low α below 0.001.[6,7] Wang and coworkers reported a high magnetoresistance (MR) ratio of 360% in a MTJ made of CFA/MgO/CFA at room temperature due to the Δ_1 band spin-filtering effect of MgO.[4] Moreover, when the thickness of the CFA film with MgO capping was reduced to 1 nm, it was reported to show PMA[8] due to the hybridization of orbitals between Fe in CFA and O in MgO.[9] Using this interfacial PMA, a perpendicular MTJ with a MgO barrier was demonstrated.[10] These reports indicate that the ultrathin CFA film with PMA is the promising ferromagnetic electrode for STT-MRAMs. However, Cui and coworkers[11] reported the magnetic damping measured by a ferromagnetic resonance (FMR) in the 1.36-nm thick CFA film with PMA to be $\alpha = 0.012$, which was ten times larger than in the thicker in-plane magnetized CFA films.[6,7] Since the large α causes the increase in J_c and α is one of the important parameters to control the magnetization dynamics, it is pressing to reveal the possible origin for the large α and how to reduce it in the ultrathin CFA films. In the present study, we estimate α by means of time-resolved magneto-optical Kerr effect (TR-MOKE) measurements under a high magnetic field that can suppress the contributions originating from the inhomogeneous effective field to the magnetization dynamics. We find α for a 1-nm thick CFA film which shows PMA to be considerably greater than those for the thicker films which exhibit in-plane anisotropy. We discuss the possible origins for the large α in the ultrathin PMA film based on the results of elemental mappings and first-principles calculations.

The samples studied were films with stacking structures of Ru(2 nm)/CFA(d)/MgO(2 nm)/Ta(2 nm)/SiN(65 nm) deposited on MgO(001) single-crystalline substrates at room temperature by magnetron sputtering with a base pressure of 4×10^{-7} Pa. The thickness d of the CFA films was varied from 1 nm to 20 nm by changing the sputtering time duration. The samples were then annealed at 325 °C in a vacuum furnace for 0.5 h, in order to achieve PMA in the ultrathin CFA films. The spin dynamics of the CFA films was estimated by TR-MOKE and FMR measurements with the magnetic field up to 2 T. For TR-MOKE, the fundamental output from a Ti:sapphire regenerative amplifier with a wavelength of 800 nm, a duration of 200 fs, and a repetition rate of 10 kHz was used as a probe, whereas the second harmonic at 400 nm was used as a pump. The pump and probe fluences were 2 and 0.15 mJ/cm^2, respectively. The pump beam was chopped at 900 Hz for the lock-in detection. The polarization rotation of the probe beam after the reflection from the sample was

a)Author to whom correspondence should be addressed: takahashi.yukiko@nims.go.jp. Tel.: +81-298-59-2719. Fax: +81-298-59-2701.

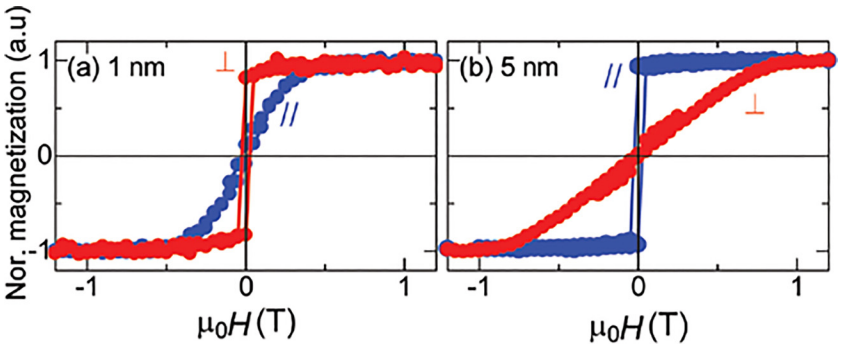

FIG. 1. Magnetization curves of the CFA samples for the thickness $d = 1$ nm (a) and 5 nm (b). Red and blue symbols correspond to the out-of-plane and in-plane directions.

detected with a pair of balanced photodetectors. For comparison, α was also estimated by means of FMR by placing the samples on a 2-port coplanar waveguide. A vector-network analyzer was used to measure the s-parameters of the waveguide at 1 GHz increments from 10 GHz to 18 GHz while a varying magnetic field ranging from 0 to 1.8 T was applied perpendicular to the film plane at each discrete frequency.[12,13] The damping parameter was extracted from the frequency dependence of the FMR linewidth. The static magnetic properties of all the samples were characterized by using a vibrating sample magnetometer (VSM) while the structure analysis was carried out by using both x-ray diffraction (XRD) and transmission electron microscopy (TEM). The XRD analysis results indicated that the CFA films had the B2 and A2 structures for $d \geq 10$ nm and $d \leq 5$ nm, respectively, as shown in the supplementary material (Fig. S1).

Figure 1 compares the out-of-plane and in-plane magnetization curves of the CFA films with the thickness of $d = 1$ and 5 nm, respectively. The sample with $d = 1$ nm shows the PMA with the anisotropy field of 0.45 T estimated from the in-plane hard axis loop, whereas that with $d = 5$ nm shows the in-plane anisotropy. The anisotropy at the MgO/CFA interface is derived to be positive at the MgO/CFA interface based on the d-dependence of K_u^{eff} d, where K_u^{eff} denotes the effective perpendicular anisotropy as shown in the supplementary material (Fig. S2). We find the CFA film with $d = 1.2$ nm also to show the PMA, whereas the films for $d \geq 5$ nm have the in-plane anisotropy.

Figure 2(a) shows the TR-MOKE signals for $d = 1$ nm under magnetic field H ranging from 0.72 to 2.0 T. The direction of H for the TR-MOKE experiments is fixed at 50° with respect to the surface normal z of the sample, as illustrated in the inset of Fig. 2(a). The excitation with a fs-laser pulse leads to an ultrafast quenching of the magnetization within 1 ps, followed by a slower recovery of the initial magnetization and precession around the applied magnetic field direction. The TR-MOKE signals after 30 ps can be fitted well to a phenomenological fitting function:

$$G = A\exp(-\nu t) + B\sin(2\pi f t + \phi)\exp\left(-\frac{t}{\tau}\right) + C. \quad (1)$$

Here, the first and third terms on the right hand side correspond to the non-oscillatory dynamics arising from the photo-excited electronic and/or lattice systems and the second to the spin precession. A and B represent amplitudes for each contribution and C is an offset. ν, f, ϕ, and τ are the decay rate of the non-oscillatory background, precession frequency, the initial phase, and relaxation time of the precession. Figures 2(b) and 2(c) show f and the inverse relaxation time $1/\tau$ as a function of H for $d = 1$ nm. We find that f increases monotonically with H, whereas $1/\tau$ exhibits a

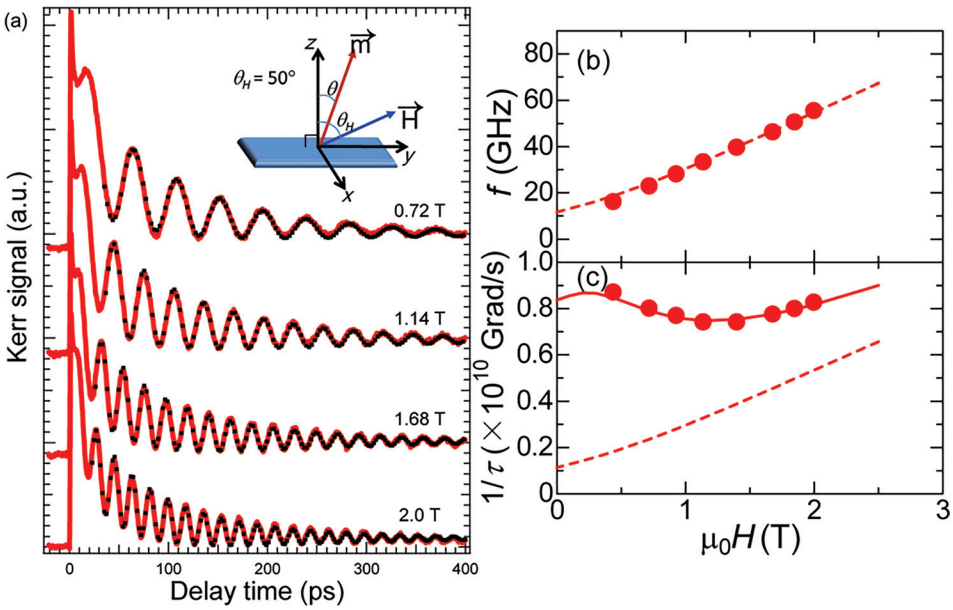

FIG. 2. (a) TR-MOKE signals from the 1-nm thick CFA film under an external magnetic field with different strengths. The black dotted curves are fits of the experimental data to Eq. (1). The inset shows the schematics of the experimental geometry. The frequency f (b) and the inverse relaxation time $1/\tau$ (c) as a function of the external magnetic field strength. The solid and broken curves are fits using the linearized LLG equation with and without including non-uniform anisotropy distribution, respectively.

shallow minimum at around 1.3 T. The spin precession frequency and the inverse relaxation time are generally derived from a linearized Landau-Lifshitz-Gilbert (LLG) equation:[14] $f = \frac{\gamma}{2\pi}\sqrt{H_1 H_2}$, $\frac{1}{\tau} = \frac{1}{2}\alpha\gamma(H_1 + H_2)$, where γ and α are the gyromagnetic ratio and damping constant. H_1 and H_2 are given by: $H_1 = H\cos(\theta_H - \theta) + H_k^{eff}\cos^2\theta$ and $H_2 = H\cos(\theta_H - \theta) + H_k^{eff}\cos 2\theta$ with θ_H and θ being the angles of H and the magnetization in the sample m with respect to z, and H_k^{eff} is an effective anisotropy field. The equilibrium angle of the magnetization is determined by $\sin 2\theta = \left(\frac{2H}{H_k^{eff}}\right)\sin(\theta - \theta_H)$. These equations lead to the monotonic increase of f and $1/\tau$ with increasing H, which in the case of $d \geq 1.2$ nm reproduced the experimentally obtained f and $1/\tau$ well, as shown in the supplementary material (Fig. S3); $\alpha = 0.011$ is obtained for $d = 1.2$ nm. In the case of $d = 1$ nm, however, the above model was far from reproducing the experimentally observed $1/\tau$, though f was reasonably reproduced, as shown in Figs. 2(b) and 2(c). To better reproduce the experimental results for $d = 1$ nm, we need to consider non-uniform distribution of the anisotropy. For this purpose, we introduce the non-uniformity $1/\tau_{ex}$ in the damping whose magnitude is expressed by ΔH_k^{eff}:[15] $\frac{1}{\tau_{ex}} = \frac{1}{2}\left|\frac{d\omega_0}{dH_k^{eff}}\right|\Delta H_k^{eff}$ with $\omega_0 = 2\pi f$. The fitting results with different values of α and ΔH_k^{eff} are compared in the supplementary material (Fig. S4). The experimental $1/\tau$ value was best reproduced by assuming $\Delta H_k^{eff} = 0.038$ T and $\alpha = 0.0155$, as shown with a solid curve in Fig. 2(c).

Figure 3 compares α obtained from TR-MOKE and FMR measurements as a function of the inverse film thickness $1/d$. Both values are comparable to what was obtained for the CFA sample in the previous study;[11] however, the value of α for $d = 1$ nm in the present study is large compared with $\alpha = 0.001$ obtained for a 50-nm thick CFA sample.[6] There is a slight difference in α for $d = 20$ nm and $\alpha = 0.003$ and 0.007 estimated by FMR and TRMOKE, respectively. With increasing $1/d$, α obtained from both techniques shows similar monotonic increases, in qualitative agreement with a previous experimental study on a CoFeB thin film[15] as well as with a calculation on Co thin films.[16] In contrast to the previous reports of the linear relationship $\alpha = \alpha_{bulk} + \alpha_{surface}/d$ for CoFeB[15] and Co,[16] possibly arising from the interface or surface effect, the present results show no clear linear relationship by $d = 1.2$ nm. In particular, the value of α for $d = 1$ nm is considerably larger than the linear extrapolation from those for larger d in the present study. Similar deviation from the linear relation was also observed for the 0.8-nm thick CoFeB sandwiched by Ta and MgO layers and attributed to the distribution of the perpendicular anisotropy originated from the thickness distribution.[15]

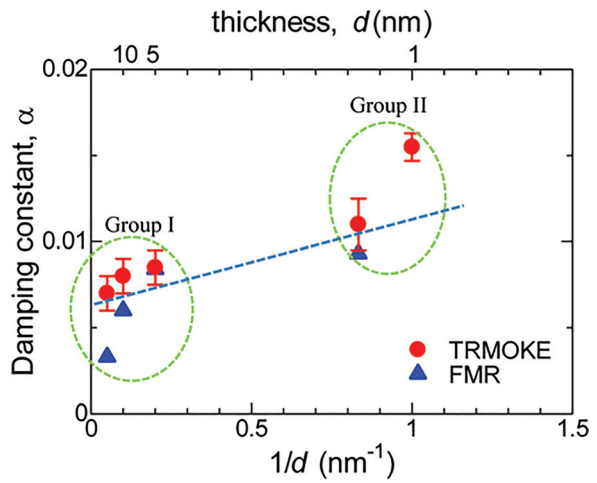

FIG. 3. The damping constant α as a function of inverse thickness $1/d$. Red and blue symbols correspond to damping constants α measured by TR-MOKE and FMR results, respectively.

A possible explanation for the rapid increase in α with increasing $1/d$ found in the present study, compared with those in the previous studies, is given specifically in terms of the non-stoichiometric composition of the CFA films due to the diffusion at the interface with MgO.[17] To check the possibility, we perform a scanning transmission electron microscope energy-dispersive-spectroscopy (STEM-EDS) analyses for $d = 1$ and 20 nm. Figure 4 compares the cross-sectional high-angle annular dark field (HAADF)-STEM images and the atomic composition line profiles for $d = 1$ and 20 nm; the corresponding elemental mappings are shown in the supplementary material (Fig. S5). We see that Al atoms near the interface significantly diffuse into MgO for both thicknesses. The nominal compositions of the whole CFA film with $d = 1$ nm and 20 nm are $Co_2Fe_{0.95}Al_{0.35}$ and $Co_2FeAl_{0.80}$, respectively. The result supports that the diffusion of Al from the CFA films is responsible for the increase in α, since this diffusion has significantly more impact on the chemical composition for thinner films. Considering the Al composition of the CFA layers, we can group these samples into two, the samples with the composition close to the stoichiometric (Group I) and those with the off-stoichiometric composition (Group II). Since the Al diffusion seriously occurs in the region within 1 nm from the interface, this grouping is

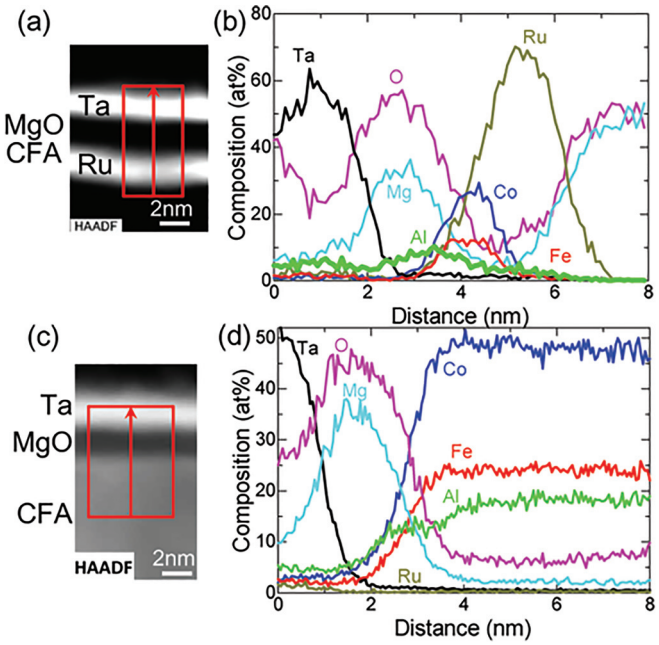

FIG. 4. Cross-sectional HAADF-STEM images (a) and (c) and the depth profiles of the atomic species (b) and (d): for $d = 1$ nm (a) and (b) and 20 nm (c) and (d). The ranges of the depth profiling are indicated by the arrows in (a) and (c).

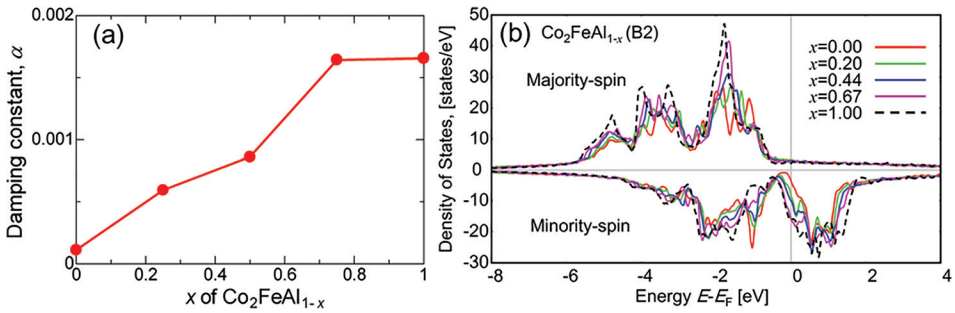

FIG. 5. Calculated α of CFA with the B2 structure at different Al compositions (a) and the corresponding spin resolved total density-of-states (b).

reasonable. The damping constants in Group II are higher than those in Group I as shown in Fig. 3.

We investigate the effect of the Al deficiency on the damping constant quantitatively by calculating α for CFA with the B2 structure at various Al compositions x in Co_2FeAl_{1-x}. First-principles density-functional calculations are performed using the Vienna *ab initio* simulation package (VASP)[18–20] and the projector augmented wave potential[21,22] including the spin-orbit interaction. We employ a torque correlation model to calculate the matrix elements of the spin-orbit-torque operator with respect to wavefunction including the spin orbit coupling.[23] A bulk simple cubic supercell of CFA with the lattice constant of 0.563 nm including 16 atoms is used, i.e., $Co_8Fe_4Al_4$ for $x = 0.0$, $Co_9Fe_4Al_3$ for $x = 0.25$, $Co_9Fe_5Al_2$ for $x = 0.50$, $Co_{10}Fe_5Al_1$ for $x = 0.75$, and $Co_{10}Fe_6$ for $x = 1.00$. We find that α increases with increasing x, as shown in Fig. 5(a). Since we consider only the energy dissipation to the electronic system through the spin-orbit interaction between local spin-moments and conductive electrons and do not include that to the phonon and spin systems due to the thermal fluctuations of the lattice and magnetic moments, the calculation results are ten times smaller than the experimental result. This kind of discrepancy is often seen in the previous papers.[24–31] However, when the Al composition changes from $x = 0.2$ to $x = 0.65$ which are obtained from the EDS analysis, the damping constant increases to about 0.001. It shows good agreement with the difference in α between Groups I and II. The spin-resolved density-of-states (DOS), shown in Fig. 5(b), also increases with increasing x in the vicinity of the Fermi level (E_F) in the minority-spin gap, because of the increase in the anti-site Co atoms at the Al-sites. Since α of 3d ferromagnetic materials is known to increase from the scattering of electrons in the d-band originating by spin-orbit coupling,[32] we expect an increase in DOS near E_F, in the local DOS of anti-site Co $d(zx)$ and $d(x^2 - y^2)$ in the minority-spin states in particular, to lead to a significant increase in α through similar scatterings. Since the change in the lattice parameter is less than 0.01 nm and Curie temperature increases with the diffusion of Al atoms from CFA, the drastic change in the energy dissipations to the spin and the phonon systems cannot be expected. Therefore, the good agreement of the difference in the damping constant between the experiment and the calculation supports our interpretation.

The experimentally observed large α for the ultrathin CFA film might also be contributed by the spin pumping effect and the interfacial spin-orbit interaction, in addition to the increase in the scattering of electrons originating from the Al deficiency in the CFA layer. In the spin pumping effect, spin current is pumped away from the interface with a non-magnetic layer through the precession in the ferromagnetic layer. This is known to have a serious impact on non-magnetic (NM) materials with strong spin-orbit coupling such as Pt.[33] At the interface between Ru and CFA, however, the spin pumping effect was found to be small[34] and MgO is also known to suppress the spin pumping effect.[35,36] We can therefore safely exclude the spin pumping effect as the possible origin of the increased damping constant. The interface can in principle modify the magnitude of PMA and thereby that of α, both of which are strongly correlated with the spin-orbit interaction. However, since PMA of the ultrathin CFA film is introduced by the hybridization of the orbitals at the interface,[9] no significant change in α is expected as a result of the change in the PMA. We therefore attribute the increase in α for the ultrathin CFA with PMA primarily to the increase in the scattering of electrons originating from the Al deficiency in the CFA layer.

In summary, we have experimentally observed an increase in α of thin CFA/MgO hetero-structured films. From the microstructure analyses, we find the significant diffusion of Al atoms near the interface of CFA and MgO layers. The samples can be grouped into two, the samples with the high α and the off-stoichiometric composition and those with low α and the stoichiometric composition. The first-principles calculations have indicated that the increase in α arises from the increase in DOS near the E_F induced by the out-diffusion of Al atoms from the CFA layer to the MgO layer. Our results have suggested that the 1-nm thick CFA film is not suitable for the application as STT-MRAM, in spite of its PMA, because of its large α. To fabricate CFA films that are more suitable for the application, deposition of more Al-rich CFA films can be a solution, so that they can reach the stoichiometric composition after the annealing and thereby achieve PMA, high P and low α. Since a high MR ratio was already reported in CFA/$MgAl_2O_4$/CFA-MTJ,[37] such chemical composition tuning is expected to lead to the realization of perpendicular MTJs with high MR ratio and low critical current for STT switching.

See supplementary material for the XRD patterns (supplementary material 1), the saturation magnetization and the effective anisotropy for various thicknesses of CFA (supplementary material 2), the magnetic field dependence of f and $1/\tau$ for $d = 1.2$ nm (supplementary material 3), and the fitting results of the magnetic field dependence of $1/\tau$ for $d = 1$ nm by changing the parameters of damping constant α and anisotropy distribution H_k^{eff} (supplementary material 4). Supplementary material 5 shows the cross-sectional high-

angle annular dark field (HAADF)-STEM images and elemental maps in the samples with $d = 1$ nm and $d = 20$ nm.

This work was in part supported by the ImPACT Program of Council for Science, Technology and Innovation, Japan. Work at UCSD supported by the National Science Foundation Award DMR No. 1312750.

[1]D. Apalkov, B. Dieny, and J. M. Slaughter, Proc. IEEE **104**, 1796 (2016).
[2]J. C. Slonczewski, J. Magn. Magn. Mater. **159**, L1 (1996).
[3]T. M. Nakatani, A. Rajanikanth, Z. Gercsi, Y. K. Takahashi, K. Inomata, and K. Hono, J. Appl. Phys. **102**, 033916 (2007).
[4]W. Wang, H. Sukegawa, and K. Inomata, Phys. Rev. B **82**, 092402 (2010).
[5]K. H. J. Buschow, P. G. van Engen, and R. Jongebreur, J. Magn. Magn. Mater. **38**, 1 (1983).
[6]S. Mizukami, D. Watanabe, M. Oogane, Y. Ando, Y. Miura, M. Shirai, and T. Miyazaki, J. Appl. Phys. **105**, 07D306 (2009).
[7]M. Belmeguenaiet, H. Tuzcuoglu, M. S. Gabor, T. Petrisor, Jr., C. Tiusan, D. Berling, F. Zighem, T. Chauveau, S. M. Cherif, and P. Moch, Phys. Rev. B **87**, 184431 (2013).
[8]Z. Wen, H. Sukegawa, S. Mitani, and K. Inomata, Appl. Phys. Lett. **98**, 242507 (2011).
[9]J. Okabayashi, H. Sukegawa, Z. Wen, K. Inomata, and S. Mitani, Appl. Phys. Lett. **103**, 102402 (2013).
[10]Z. Wen, H. Sukegawa, T. Furubayashi, J. Koo, K. Inomata, S. Mitani, J. P. Hadorn, T. Ohkubo, and K. Hono, Adv. Mater. **26**, 6483 (2014).
[11]Y. Cui, B. Khodadadi, S. Schafer, T. Mewes, J. Lu, and T. A. Wolf, Appl. Phys. Lett. **102**, 162403 (2013).
[12]C. Bilzer, T. Devolder, P. Crozat, and C. Chappert, J. Appl. Phys. **101**, 074505 (2007).
[13]D. H. Kim, H. H. Kim, C.-Y. You, and H.-S. Kim, J. Magn. **16**, 206 (2011).
[14]S. Mizukami, F. Wu, A. Sakuma, J. Walowski, S. Watanabe, T. Kubota, X. Zhang, H. Naganuma, M. Oogane, Y. Ando, and T. Miyazaki, Phys. Rev. Lett. **106**, 117201 (2011).
[15]S. Iihama, S. Mizukami, H. Naganuma, M. Oogane, Y. Ando, and T. Miyazaki, Phys. Rev. B **89**, 174416 (2014).
[16]E. Barati, M. Cinal, D. M. Edwards, and A. Umerski, EPJ Web Conf. **40**, 18003 (2013).
[17]Z. C. Wen, J. P. Hadorn, J. Okabayashi, H. Sukegawa, T. Ohkubo, K. Inomata, S. Mitani, and K. Hono, Appl. Phys. Express **10**, 013003 (2017).
[18]G. Kresse and J. Hafner, Phys. Rev. B **47**, 558 (1993).
[19]G. Kresse and J. Furthmüller, Comput. Mater. Sci. **6**, 15 (1996).
[20]G. Kresse and J. Furthmüller, Phys. Rev. B **54**, 11169 (1996).
[21]P. E. Blőchl, Phys. Rev. B **50**, 17953 (1994).
[22]G. Kresse and D. Joubert, Phys. Rev. B **59**, 1758 (1999).
[23]V. Kambersky, Czech. J. Phys. B **26**, 1366 (1976).
[24]R. Yilgin, M. Oogane, Y. Ando, and T. Miyazaki, J. Magn. Magn. Mater. **310**, 2322 (2007).
[25]M. Oogane, T. Kubota, Y. Kota, S. Mizukami, H. Naganuma, A. Sakuma, and Y. Ando, Appl. Phys. Lett. **96**, 252501 (2010).
[26]F. J. Yang and X. Q. Chen, Appl. Phys. Lett. **102**, 252407 (2013).
[27]M. Oogane, T. Kubota, H. Naganuma, and Y. Ando, J. Phys. D: Appl. Phys. **48**, 164012 (2015).
[28]S. Andrieu, A. Neggache, T. Hauet, T. Devolder, A. Hallal, M. Chshiev, A. M. Bataille, P. LeFevre, and F. Bertran, Phys. Rev. B **93**, 094417 (2016).
[29]C. Liu, C. K. A. Mewes, M. Chshiev, T. Mewes, and W. H. Butler, Appl. Phys. Lett. **95**, 022509 (2009).
[30]A. Sakuma, J. Phys. D: Appl. Phys. **48**, 164011 (2015).
[31]B. Pradines, R. Arras, I. Abdallah, N. Biziere, and L. Calmels, Phys. Rev. B **95**, 094425 (2017).
[32]V. Kambersky, Can. J. Phys. **48**, 2906 (1970).
[33]S. Mizukami, H. Abe, D. Watanabe, M. Oogane, Y. Ando, and T. Miyazaki, Appl. Phys. Express **1**, 121301 (2008).
[34]Z. C. Wen, J. Kim, H. Sukegawa, M. Hayashi, and S. Mitani, AIP Adv. **6**, 056307 (2016).
[35]A. Ruiz-Calaforra, T. Bracher, V. Lauer, P. Pirro, B. Heinz, M. Geilen, A. V. Chumak, A. Conca, B. Leven, and B. Hillebrands, J. Appl. Phys. **117**, 163901 (2015).
[36]M. Konoto, H. Imanura, T. Taniguchi, K. Yakushiji, H. Kubota, A. Fukushima, K. Ando, and S. Yuasa, Appl. Phys. Express **6**, 073002 (2013).
[37]T. Scheike, H. Sukegawa, T. Ohkubo, S. Mitani, and K. Hono, Appl. Phys. Express **9**, 053004 (2016).